Probing the antibody-catalyzed water-oxidation pathway at atomic resolution

Xueyong Zhu[†], Paul Wentworth, Jr.[‡§], Anita D. Wentworth[‡], Albert Eschenmoser[†¶‖], Richard A. Lerner[†‡§¶], and Ian A. Wilson[†§¶]

Departments of [†]Molecular Biology and [‡]Chemistry and [¶]The Skaggs Institute for Chemical Biology, The Scripps Research Institute, 10550 North Torrey Pines Road, La Jolla, CA 92037; and [‖]Laboratorium für Organische Chemie, Eidgenössische Technische Hochschule Hönggerberg HCl-H309, Universitätstrasse 16, CH-8093 Zurich, Switzerland

Contributed by Richard A. Lerner, December 19, 2003

Antibodies can catalyze the generation of hydrogen peroxide (H_2O_2) from singlet dioxygen ($^1O_2^*$) and water via the postulated intermediacy of dihydrogen trioxide (H_2O_3) and other trioxygen species. Nine different crystal structures were determined to elucidate the chemical consequences to the antibody molecule itself of exposure to such reactive intermediates and to provide insights into the location on the antibody where these species could be generated. Herein, we report structural evidence for modifications of two specific antibody residues within the interfacial region of the variable and constant domains of different murine antibody antigen-binding fragments (Fabs) by reactive species generated during the antibody-catalyzed water oxidation process. Crystal structure analyses of murine Fabs 4C6 and 13G5 after UV-irradiation revealed complex oxidative modifications to tryptophan L163 and, in 4C6, hydroxylation of the C^γ of glutamine H6. These discrete modifications of specific residues add further support for the "active site" of the water-oxidation pathway being located within the interfacial region of the constant and variable domains and highlight the general resistance of the antibody molecule to oxidation by reactive oxygen species generated during the water-oxidation process.

crystal structure | amino acid modification | reactive oxygen species | oxidative damage | UV-irradiation

Antibodies, regardless of source or antigenic specificity, can catalyze the generation of multimolar equivalents of hydrogen peroxide (H_2O_2) from singlet dioxygen ($^1O_2^*$) and water (1) via the postulated intermediacy of dihydrogen trioxide (H_2O_3) (2). Activation of this process by photochemical sensitizers and visible light leads to highly efficient killing of bacteria, wherein the antibody-catalyzed water-oxidation pathway appears to generate an additional oxidant with a chemical signature similar to that of ozone (O_3) (3). More recently, we reported that this process regioselectively converted antibody antigen-binding fragment (Fab) 4C6-bound benzoic acid into *para*-hydroxybenzoic acid, as well as regioselectively hydroxylating the 4-position of the indole of a single tryptophan residue, L163, within the 4C6 Fab structure (4).

A number of structural questions remain to be answered regarding the ability of antibodies to catalyze this biologically unique oxidation pathway. First, where is the location of the active site in which $^1O_2^*$ and H_2O react, and second, what are any oxidative consequences to the antibody molecule itself as a result of carrying out this reaction? To understand these issues, we determined a series of x-ray structures from Fab fragments of antibodies that were previously used to document the water-oxidation pathway.

Materials and Methods

UV-Irradiation of Fab Fragments. Murine Fab fragments were generated and purified as previously described for 4C6 (5) and 13G5 (6). To obtain UV-irradiated Fabs, purified 4C6 Fab (200 μl, 26 mg/ml in 0.1 M sodium acetate buffer, pH 5.5) or 13G5 Fab (200 μl, 15 mg/ml in PBS, pH 7.4) were irradiated on a transilluminator with UV light (312 nm, 0.8 mW·cm^{-2}) for 30 min at room temperature.

Hydrogen Peroxide Soaking Experiments. An aqueous solution of H_2O_2 (final concentration 3 mM) was added to a crystal of the native 4C6 Fab grown from 15% (wt/vol) polyethylene glycol (PEG) 4000/0.2 M sodium acetate/0.1 M Tris·HCl, pH 8.5. The crystal was allowed to react for 3 min at room temperature before being flash-cooled and stored in liquid nitrogen.

Crystallization Conditions. Crystallization experiments were performed by using the sitting-drop vapor-diffusion method at 295 K with a drop consisting of 1 μl of reservoir solution and 1 μl of protein solution. For 4C6 Fab, UV-irradiated 4C6 Fab crystal **1** (see Table 1) and the native 4C6 Fab crystal **2** were grown from 15% (wt/vol) PEG 4000/0.2 M ammonium acetate/0.1 M sodium acetate, pH 4.6. The UV-irradiated 4C6 crystal **3** and the native 4C6 crystal **4** (5) were grown from 15% (wt/vol) PEG 4000/0.2 M ammonium acetate/0.1 M trisodium citrate, pH 5.6, whereas native 4C6 crystals **5** and **6** arose from 15% (wt/vol) PEG 4000/0.2 M sodium acetate/0.1 M Tris·HCl, pH 8.5. For 13G5 Fab, UV-irradiated 13G5 crystal **7** and native 13G5 crystal **8** were grown from 20% (wt/vol) PEG 3000/0.2 M zinc acetate/5–7% (vol/vol) isopropyl alcohol/0.1 M imidazole, pH 8.0.

Data Collection and Processing. Crystals of 4C6 Fab for data sets A–G were cryocooled in liquid nitrogen after soaking in mother liquid substituted with 25% (vol/vol) glycerol. Crystals of 13G5 Fab for data sets H and I were flash-cooled in liquid nitrogen with 20% (vol/vol) glycerol as cryoprotectant. All of the data sets were integrated and scaled with HKL2000 (7) (see Tables 1 and 2).

For the UV-irradiated 4C6 crystal **1**, data set A was collected in-house on a MAR Research image plate detector (diameter 300 mm) mounted on a Rigaku x-ray generator (50 kV, 70 mA) as described (4). A second data set, B, was also collected from this crystal **1** at the Stanford Synchrotron Radiation Laboratory (SSRL) beamline 11-1. A native 4C6 crystal **2**, data set C, was collected as a control for data sets A and B at SSRL beamline 9-1. For the UV-irradiated 4C6 crystal **3**, data set D was collected at SSRL beamline 11-1, whereas the control native 4C6 crystal **4** data set E was collected at the Advanced Light Source (ALS) as described (5). For the H_2O_2-soaked 4C6 crystal **5**, data

Abbreviations: Fab, antibody antigen-binding fragment; PEG, polyethylene glycol; SSRL, Stanford Synchrotron Radiation Laboratory.

Data deposition: The six structures and structure factors of 4C6 Fab and two structures and structure factors of 13G5 Fab have been deposited at the Protein Data Bank, www.rcsb.org (PDB ID codes 1ru9, 1rua, 1ruk, 1rul, 1rum, 1rup, 1ruq, and 1rur, respectively).

[§]To whom correspondence may be addressed. E-mail: wilson@scripps.edu, paulw@scripps.edu, or foleyral@scripps.edu.

Table 1. Data collection and refinement statistics for UV-irradiated, H_2O_2-soaked, and native 4C6 Fab crystals

	Data set						
	A UV-irradiated	B UV-irradiated	C Native	D UV-irradiated	E* Native	F H_2O_2-soaked	G Native
Crystal no.	**1**	**1**	**2**	**3**	**4**	**5**	**6**
Space group	$P4_12_12$	$P4_12_12$	$P4_12_12$	$P4_12_12$	$P4_12_12$	$P4_12_12$	$P4_12_12$
Unit cell, Å	$a = b = 64.1$ $c = 266.0$	$a = b = 64.1$ $c = 266.3$	$a = b = 64.1$ $c = 266.3$	$a = b = 63.9$ $c = 265.7$	$a = b = 64.1$ $c = 265.6$	$a = b = 64.4$ $c = 267.0$	$a = b = 64.2$ $c = 266.5$
Resolution, Å†	50.0–2.50 (2.54–2.50)	50.0–1.75 (1.78–1.75)	50.0–1.40 (1.42–1.40)	50.0–1.88 (1.92–1.88)	50.0–1.30 (1.32–1.30)	50.0–1.48 (1.52–1.48)	50.0–1.40 (1.43–1.40)
Beamline	In-house	SSRL 11–1	SSRL 9–1	SSRL 11–1	ALS 5.0.2	SSRL 9–1	APS 19-ID
No. of unique reflections	18,691	57,518	111,974	42,866	117,957	92,687	104,925
Redundancy	3.6	6.3	4.6	5.1	3.9	3.8	7.2
Average $I/\sigma(I)$†	12.3 (2.0)	31.7 (2.9)	38.7 (2.4)	22.6 (1.4)	26.3 (1.5)	29.6 (1.4)	31.4 (2.4)
Completeness, %†	92.0 (90.9)	99.8 (99.9)	99.7 (99.4)	90.7 (72.4)	86.0 (69.6)	97.8 (98.8)	93.4 (90.7)
R_{sym}‡	0.091	0.062	0.044	0.080	0.041	0.070	0.079
No. of protein atoms	3,382	3,382	3,380	3,382	3,380	3,381	3,380
No. of solvent molecules	242	427	429	341	577	625	474
R_{cryst}§	0.192	0.194	0.166	0.206	0.158	0.175	0.161
R_{free}¶	0.247	0.251	0.210	0.283	0.208	0.245	0.212
Average *B* values, Å^2	30.0	31.0	22.7	34.5	20.6	24.9	22.6
rmsd bond lengths, Å	0.012	0.008	0.011	0.006	0.013	0.012	0.013
rmsd bond angles, °	1.6	2.1	2.2	1.9	2.3	2.2	2.3

ALS, Advanced Light Source; APS, Advanced Photon Source; rmsd, rms deviation.
*The data statistics for published data set E (5) are shown here for comparison.
†Parentheses denote outer-shell statistics.
‡$R_{sym} = \Sigma_h\Sigma_i|I_i(h) - \langle I(h)\rangle|/\Sigma_h\Sigma_i I_i(h)$, where $\langle I(h)\rangle$ is the average intensity of *i* symmetry-related observations of reflections with Bragg index *h*.
§$R_{cryst} = \Sigma_{hkl}||F_o| - |F_c|/\Sigma_{hkl}|F_o|$, where F_o and F_o are the observed and calculated structure factors.
¶R_{free} was calculated as for R_{cryst}, but on 5% of data excluded before refinement.

set F was collected at SSRL beamline 9-1, and its control native 4C6 crystal **6** data set G was collected on an attenuated beamline 19-ID at the Advanced Photon Source (APS).

The UV-irradiated 13G5 crystal **7** data set H was collected in-house on a Mar detector (diameter 345 mm) mounted on a Siemens x-ray generator (50 kV, 100 mA), and its control native 13G5 crystal **8** data set I was collected at SSRL beamline 9-1.

Crystallographic Refinement. For all data sets of 4C6 Fab, CNS (8) was used for rigid-body refinement, using the published native crystal structure E (PDB ID code 1ncw) as the initial model (5). Data set A was refined only with CNS, whereas refinements of all other structures were completed with SHELXL (9) (see Table 1). Anisotropic *B*-value refinement was applied to high-resolution data sets C, E, F, and G. The 13G5 Fab-inhibitor complex (PDB ID code 1a3l) (6) was used as the initial model for rigid-body refinement of the 13G5 data sets by using CNS (8). Data set H was refined only with CNS (8) (see Table 2), whereas high-resolution structure I was completed with SHELXL (9), using anisotropic *B*-value refinement (see Table 2). In all 4C6 and 13G5 Fab structures, Trp^{L163} was initially modeled and refined as alanine to avoid any potential bias in the electron-density maps. In UV-irradiated 4C6 Fab structures A, B, and D and H_2O_2-soaked 4C6 Fab structure F, Trp^{L163} was also refined as 4-hydroxytryptophan, and Gln^{H6} as γ-hydroxyglutamine except in the H_2O_2-soaked 4C6 Fab structure F. Model rebuilding was performed by using O (10).

Results

Modification of Trp^{L163} of 4C6 Fab. Comparison of the UV-irradiated (A) and native (C) 4C6 Fab structures at 2.50- and 1.40-Å resolution, respectively, showed no discernible changes in their main-chain conformations (rms deviation 0.25 Å) (Fig. 1). However, closer inspection revealed that one particular tryptophan, Trp^{L163}, and one glutamine, Gln^{H6}, were consistently modified upon UV-irradiation of 4C6 Fab (Fig. 1, compare data sets A and C). The structural modifications were interpreted as regioselective hydroxylation of the 4-position as well as reduced definition at the 1-position of the indole of Trp^{L163}, and as γ-hydroxylation of Gln^{H6} (Fig. 2 *aA*, *bA*, *cA*, and *dA* and Fig. 3 *aA*, *bA*, *cA*, and *dA*, respectively). Analysis of the higher 1.75-Å resolution structure B collected at a synchrotron source from the same crystal **1** as structure A revealed that Trp^{L163} had been modified more severely (Fig. 2 *aB*, *bB*, *cB*, and *dB*). The modification involved an apparent fragmentation at a locus between the 4- and 7-positions of the phenyl ring of the tryptophan indole; no modification of Trp^{L163} (Fig. 2 *aC*, *bC*, *cC*, and *dC*) was detected in the control native data set C with crystal **2** that was collected at the same synchrotron source (Table 1).

This extensive modification of Trp^{L163} was also apparent in electron density maps from the 1.88-Å resolution data set D

Table 2. Data collection and refinement statistics for UV-irradiated and native 13G5 Fab

	Data set	
	H UV-irradiated	I Native
Crystal no.	**7**	**8**
Space group	*C*2	*C*2
Unit cell, Å	$a = 179.9$, $b = 40.5$, $c = 68.0$	$a = 179.3$, $b = 40.3$, $c = 67.6$
Unit cell, °	$\beta = 110.0$	$\beta = 109.9$
Resolution, Å	50.0–1.86 (1.93–1.86)	50.0–1.50 (1.53–1.50)
Beamline	In-house	SSRI 9–1
No. of unique reflections	36,527	71,213
Redundancy	3.7	2.7
Average $I/\sigma(I)$	24.2 (1.4)	24.0 (1.6)
Completeness, %	93.7 (60.0)	97.4 (97.9)
R_{sym}	0.064	0.047
No. of protein atoms	3,308	3,308
No. of solvent molecules	362	372
R_{cryst}	0.219	0.191
R_{free}	0.256	0.256
Average B values, Å^2	33.4	25.8
rmsd bond lengths, Å	0.006	0.008
rmsd bond angles, °	1.4	2.0

See footnotes to Table 1.

(Fig. 2 *aD*, *bD*, *cD*, and *dD*), also collected at the SSRL beamline 11-1 from a second UV-irradiated 4C6 Fab crystal **3** that had been obtained under different crystallization conditions. It should be noted that, in contrast to crystal **1**, crystal **3** was not previously irradiated on the in-house x-ray facility. Again, no structural modifications were observed with the control native 4C6 Fab crystal **4** (Fig. 2 *aE*, *bE*, *cE*, and *dE*).

Similar observations were made for the H_2O_2-soaked 4C6 crystals. Fab crystal **5** at 1.48 Å (data set F) also revealed that the overall backbone structure of the H_2O_2-soaked 4C6 Fab had no discernible changes relative to the native structure (data set G). However, the side chain of Trp^{L163} was also modified in the H_2O_2-soaked crystal **5** (Fig. 2 *aF*, *bF*, *cF*, and *dF*) relative to the control native 4C6 Fab (Fig. 2 *aG*, *bG*, *cG*, and *dG*). The H_2O_2-induced modifications to Trp^{L163} (data set F) were similar to those observed with UV-irradiated 4C6 structures B (Fig. 2 *aB*, *bB*, *cB*, and *dB*) and D (Fig. 2 *aD*, *bD*, *cD*, and *dD*). An additional modification, unique to data set F, occurred with the antigen-binding site Trp^{H97} (see Fig. 1) that also appeared to be oxidized with low occupancy but at the 7-position of the indole (data not shown). No other discernible chemical changes in the remaining tryptophan residues were detected in any 4C6 Fab data sets. However, several other solvent-exposed residues had possible chemical modifications in the H_2O_2-soaked 4C6 crystals, including the side chains of Gln^{L38}, Gln^{L42}, Asp^{L60}, Tyr^{L87}, Asp^{H72}, and Asp^{H99}, although this effect appeared to be only partial (data not shown) with some correlation between solvent accessibility and susceptibility of the individual amino acid to modification.

Modification of Gln^{H6} of 4C6 Fab. In the UV-irradiated 4C6 Fab crystal structure A, additional spherical density proximal to the side-chain C^{γ} of Gln^{H6} was revealed from a difference Fourier map (Fig. 3*dA*). This density was not present in maps from several other data sets collected from native 4C6 Fab crystals (such as in Fig. 3 *dC* and *dE*). This additional electron density was also found in the maps calculated from data sets B (Fig. 3*dB*) and D (Fig. 3*dD*). A hydroxyl group was modeled into the density and refined to an occupancy factor of ≈60–80% in data sets A, B, and D. Interestingly, no hydroxylation of Gln^{H6} was observed from the H_2O_2-soaked 4C6 Fab data set F.

Modification of Trp^{L163} of 13G5 Fab. Comparison of the UV-irradiated (H) and native (I) 13G5 Fab structures at 1.86- and 1.50-Å resolution, respectively, showed no discernible difference in their main-chain structures (data not shown). Only

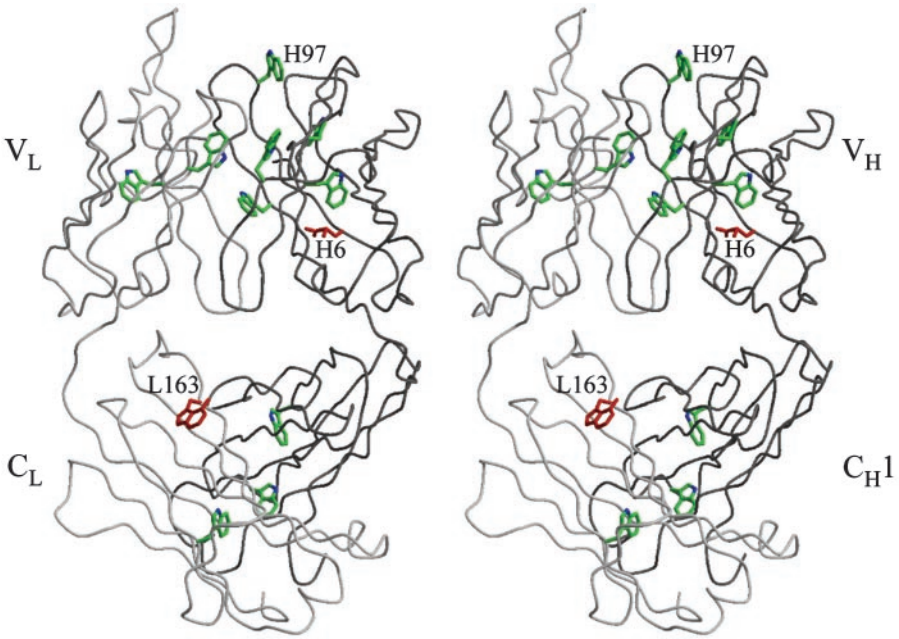

Fig. 1. Stereoview of the crystal structure of 4C6 Fab, with the C^{α} trace of the light (L) and heavy (H) chains colored in light and dark gray, respectively. The modified tryptophan Trp^{L163} is highlighted in red, and other tryptophan residues (such as Trp^{H97}) are colored green. The modified glutamine residue Gln^{H6} is also colored red. All of the figures were generated in BOBSCRIPT (12) and rendered in RASTER3D (13).

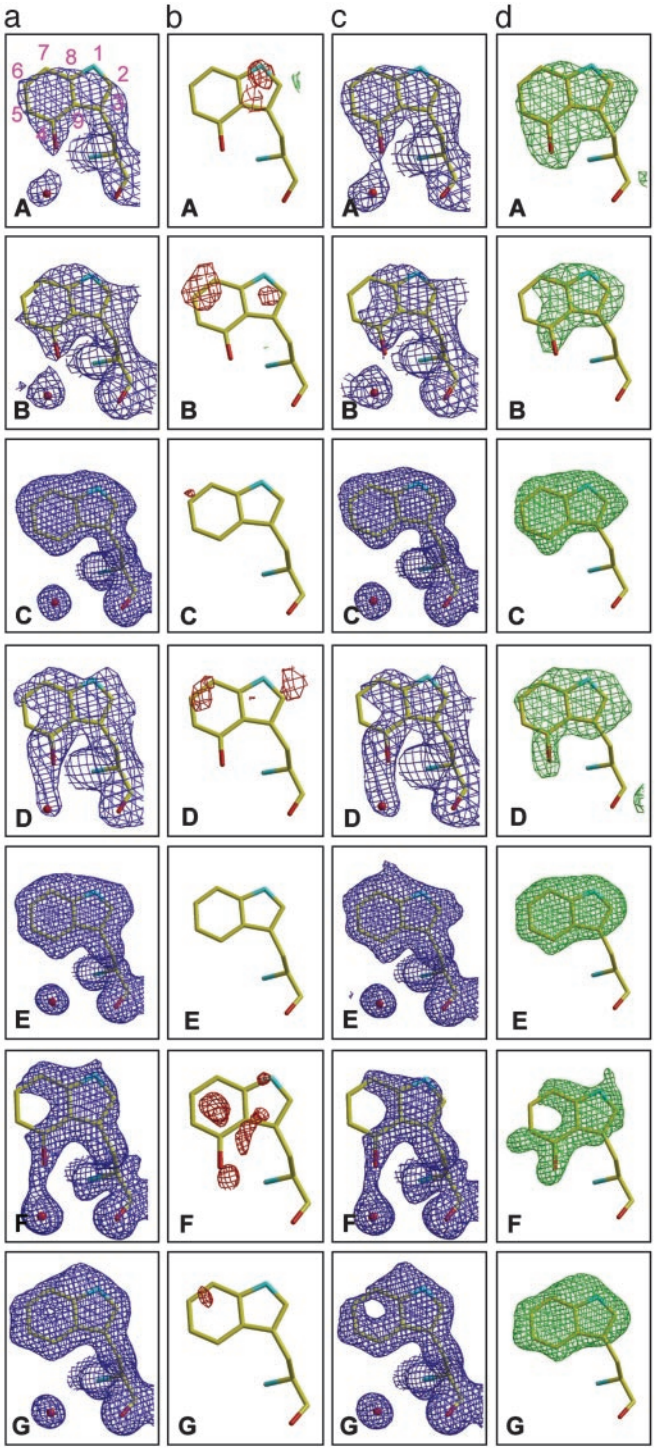

Fig. 2. Fourier electron density maps for Trp^{L163} in 4C6 Fab: the UV-irradiated data set A, the UV-irradiated data set B, the native control data set C, the UV-irradiated data set D, the native control data set E, the H_2O_2-soaked data set F, and the native control data set G. For *a* and *b*, the tryptophan was modeled and refined as 4-hydroxytryptophan for data sets A, B, D, and F and was modeled and refined as tryptophan for control data sets C, E, and G. As a control (*c* and *d*), the tryptophan residue was modeled and refined as alanine to avoid model bias. (*a*) $2F_o - F_c$ maps (blue), contoured at 1.0 σ. (*b*) $F_o - F_c$ maps, contoured at 2.5 σ (green) and -2.5 σ (red) for data sets A, B, and D and contoured at 3.0 σ (green) and -3.0 σ (red) for data sets C, E, F, and G. (*c*) $2F_o - F_c$ maps (blue), contoured at 0.8 σ for data sets A, B, C, D, and E, and contoured at 0.9 σ for data sets F and G. (*d*) $F_o - F_c$ maps, contoured at 2.5 σ (green) for data sets A, B, and D, and contoured at 3.0 σ (green) for data sets C, E, F, and G.

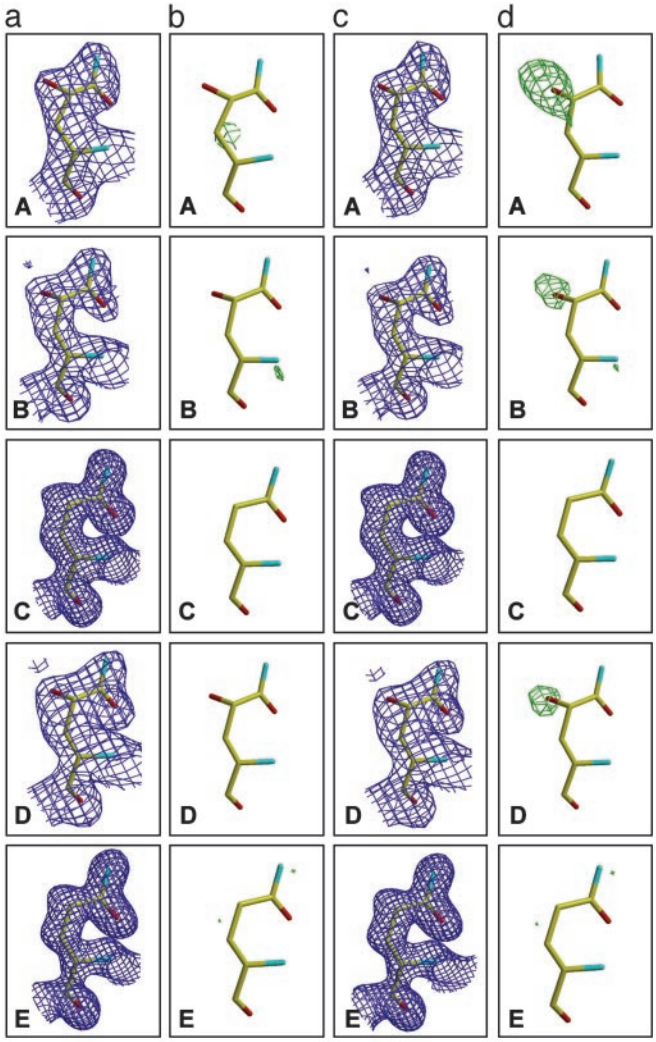

Fig. 3. Fourier electron density maps around Gln^{H6} in 4C6 Fab: for data sets A to E as described for Fig. 2. For *a* and *b*, the glutamine residue was modeled and refined as γ-hydroxyglutamine for data sets A, B, and D and modeled and refined as glutamine for control data sets C and E. As a control (*c* and *d*), the glutamine residue was modeled and refined as glutamine for all data sets. (*a*) $2F_o - F_c$ maps (blue), contoured at 1.0 σ. (*b*) $F_o - F_c$ maps, contoured at 3.0 σ (green) and -3.0 σ (red). (*c*) $2F_o - F_c$ maps (blue), contoured at 1.0 σ. (*d*) $F_o - F_c$ maps, contoured at 3.0 σ (green).

oxidative modifications to Trp^{L163} were apparent in structure H, which was determined from an in-house data set (Fig. 4 *aH*, *bH*, *cH*, and *dH*). The 1-, 2-, and 8-positions of the indole of the Trp^{L163} have reduced definition in the electron density maps relative to that of the control structure I (Fig. 4 *aI*, *bI*, *cI*, and *dI*). Trp^{L163} is located in the constant region of 13G5 Fab light chain, and is in a position similar to that in the 4C6 Fab. No modifications were observed for the H6 residue in UV-irradiated 13G5 Fab, which is, in this case, glutamate instead of glutamine as in 4C6 Fab.

Discussion

The key conclusion from this study is that only very few modifications occur in antibodies upon irradiation with UV light and, by assumption, during processing of $^1O_2^*$ into H_2O_2. This structural observation supports our kinetic investigations, which show that antibodies continue to catalyze the water-oxidation pathway with no apparent reduction in activity even after several

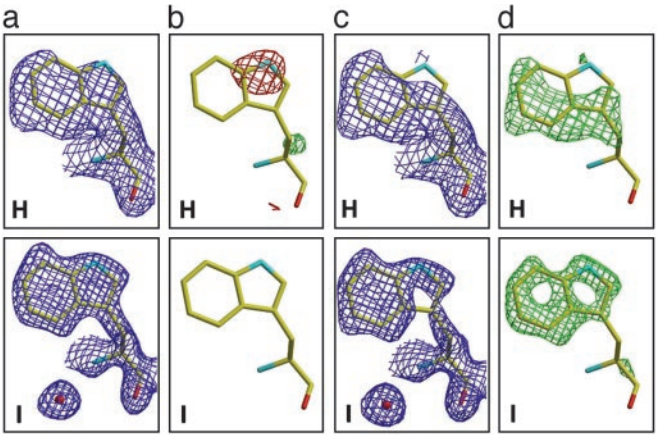

Fig. 4. Fourier electron density maps showing Trp^{L163} in 13G5 Fab for UV-irradiated data set H and native control data set I. For *a* and *b*, the tryptophan residue was refined as tryptophan, whereas for control (*c* and *d*), the tryptophan residue was refined as alanine to avoid model bias. (*a*) $2F_o - F_c$ maps (blue), contoured at 1.0 σ. (*b*) $F_o - F_c$ maps, contoured at 3.0 σ (green) and -3.0 σ (red). (*c*) $2F_o - F_c$ maps (blue), contoured at 0.8 σ. (*d*) $F_o - F_c$ maps, contoured at 3.0 σ (green).

hours of UV-irradiation (2). However, one residue, Trp^{L163}, is consistently modified during UV-irradiation and is a highly conserved in murine antibodies. The Trp^{L163} residue is located in the constant domain of the light chain, and its side chain projects into the interfacial region between the variable and constant domains. Of the 11 tryptophan residues within 4C6 Fab, Trp^{L163} is the only one modified in the water-oxidation process. Trp^{L163} is the most solvent-accessible of all of the 4C6 tryptophan residues, with a solvent-accessible surface area of 113 $Å^2$ (1.4-Å probe radius). However, it is unlikely that exposure to solvent is the sole reason for its modification, given that most of the other tryptophan residues have some solvent exposure. For example, no measurable modifications occurred on Typ^{H97}, which is located atop the antigen-binding site and is only slightly less solvent accessible (100 $Å^2$) (Fig. 1).

Nevertheless, the nature of the structural modifications to Trp^{L163} in the Fabs 4C6 and 13G5 is quite different. In the 4C6 Fab, the 4-position of the indole appears to be hydroxylated and, upon synchrotron x-ray irradiation, an apparent fragmentation occurs at a locus between the 4- and 7-positions of the 4-hydroxyphenyl ring of the indole. In the 13G5 Fab structure, it is the indole's pyrrole ring that is disrupted.

Gln^{H6} is located in the variable domain of the heavy chain of the 4C6 Fab with its side chain buried in a hydrophobic core, but close to the interfacial region of the constant and variable domains (Fig. 1). Gln^{H6} appears to be hydroxylated at the γ-position in the UV-irradiated 4C6 crystal structures (A, B, and D). For 13G5 Fab, however, H6 is a glutamate instead of glutamine residue, and no modification was found.

Chemical modification of tryptophan in aqueous systems by the hydroxyl radical ($HO^{\bullet}$), generated either by pulsed radiolysis of water or by Fenton chemistry, leads to a complex mixture of products that includes *N*-formylkynurenine, multiple hydroxylation products, and fragmentation products (11). Much less is known about the chemical products of glutamine and $HO^{\bullet}$; however, γ-hydroxylation is an entirely reasonable modification. Thus, the combined analyses of the structural modifications to Trp^{L163} in both the 4C6 and 13G5 Fabs and the regioselective hydroxylation of Gln^{H6} in the 4C6 Fab strengthen the evidence for generation of a hydroxyl radical (or a surrogate such as the hydrotrioxy radical) in the antibody-catalyzed water-oxidation pathway.

The hydrogen peroxide soaking experiment was undertaken to investigate the possible location of the active site for the water-oxidation pathway in antibodies. Hydrogen peroxide is the stable product of the antibody-catalyzed water-oxidation process and is known to inhibit (IC_{50} $\approx$500 μM) the overall process by presumed binding within the putative catalytic site (2). Therefore, it was surmised that, if a discrete binding site existed, H_2O_2 would be sequestered within the active site by soaking the crystal of 4C6 Fab in an H_2O_2 solution at a concentration well above its IC_{50}. Given that x-ray irradiation of H_2O_2, even at liquid nitrogen temperatures, generates hydroxyl radicals, it was anticipated that during the in-house/synchrotron x-ray analysis of the H_2O_2-soaked crystals that residues in or close to the active site could become hydroxylated.

The H_2O_2 crystal soaking experiment revealed clear evidence that Trp^{L163} was indeed modified (with a high occupancy, >80–90%) within the 4C6 Fab structure. The nature of the modification was very similar to that observed when the 4C6 Fab was treated with UV-irradiation, i.e., when the water-oxidation pathway was activated, the phenyl ring of the indole side chain was fragmented.

Thus, evidence for structural modifications of Trp^{L163} in different Fabs by UV-irradiation supports the proposal that Trp^{L163} is located close to the site of reactive oxygen species generated during the antibody-catalyzed water-oxidation pathway and that the precise locus and nature of the modification to the side chain is entirely dependent upon the indole side chain's orientation and localized environment with respect to the attacking species. Furthermore, the H_2O_2 crystal soaking experiment supports the notion that the active site for the antibody-catalyzed water-oxidation pathway is situated at or near the interfacial region of the variable and constant domains and that its locus is in close proximity to Trp^{L163}.

The antibody-catalyzed water-oxidation pathway is a complex cascade initiated by singlet oxygen, ultimately generating hydrogen peroxide. A cascade of intermediates have been postulated to include dihydrogen trioxide, ozone, and even hydroxyl radical surrogates, such as the hydrotrioxy radical ($HO_3^{\bullet}$). This study provides the strongest evidence yet for the structural location of the active site of this highly conserved process as being in the interfacial region of the variable and constant domains. Furthermore, the relatively small number of structural modifications to side-chain residues in the antibody after activation of the water-oxidation pathway reinforces the remarkable ability of these proteins to handle reactive oxygen species in a manner that does not lead to their rapid destruction.

We thank the staffs of the Stanford Synchrotron Radiation Laboratory beamlines BL9-1 and BL11-1, the Advanced Photon Source beamline 19-ID, and the Advanced Light Source beamline 5.0.2, and several lab members, especially Dr. Xiaoping Dai, for help with data collection. We are grateful to Dr. Kim D. Janda for antibody samples. This work was supported by National Institutes of Health Grant CA27489 (to I.A.W. and R.A.L.) and The Skaggs Institute for Chemical Biology. This is manuscript no. 16245-MB of The Scripps Research Institute.

1. Wentworth, A. D., Jones, L. H., Wentworth, P., Janda, K. D. & Lerner, R. A. (2000) *Proc. Natl. Acad. Sci. USA* **97,** 10930–10935.
2. Wentworth, P., Jones, L. H., Wentworth, A. D., Zhu, X. Y., Larsen, N. A., Wilson, I. A., Xu, X., Goddard, W. A., Janda, K. D., Eschenmoser, A. & Lerner, R. A. (2001) *Science* **293,** 1806–1811.
3. Wentworth, P., McDunn, J. E., Wentworth, A. D., Takeuchi, C., Nieva, J., Jones, T., Bautista, C., Ruedi, J. M., Gutierrez, A., Janda, K. D., *et al*. (2002) *Science* **298,** 2195–2199.
4. Wentworth, P., Wentworth, A. D., Zhu, X. Y., Wilson, I. A., Janda, K. D., Eschenmoser, A. & Lerner, R. A. (2003) *Proc. Natl. Acad. Sci. USA* **100,** 1490–1493.
5. Zhu, X. Y., Heine, A., Monnat, F., Houk, K. N., Janda, K. D. & Wilson, I. A. (2003) *J. Mol. Biol.* **329,** 69–83.

6. Heine, A., Stura, E. A., Yli-Kauhaluoma, J. T., Gao, C. S., Deng, Q. L., Beno, B. R., Houk, K. N., Janda, K. D. & Wilson, I. A. (1998) *Science* **279,** 1934–1940.
7. Otwinowski, Z. & Minor, W. (1997) *Methods Enzymol.* **276,** 307–326.
8. Brünger, A. T., Adams, P. D., Clore, G. M., DeLano, W. L., Gros, P., Grosse-Kunstleve, R. W., Jiang, J. S., Kuszewski, J., Nilges, M., Pannu, N. S., *et al.* (1998) *Acta Crystallogr. D* **54,** 905–921.
9. Sheldrick, G. M. & Schneider, T. R. (1997) *Methods Enzymol.* **277,** 319–343.
10. Jones, T. A., Zou, J. Y., Cowan, S. W. & Kjeldgaard, M. (1991) *Acta Crystallogr. A* **47,** 110–119.
11. Maskos, Z., Rush, J. D. & Koppenol, W. H. (1992) *Arch. Biochem. Biophys.* **296,** 514–520.
12. Esnouf, R. M. (1999) *Acta Crystallogr. D* **55,** 938–940.
13. Merritt, E. A. & Murphy, M. E. P. (1994) *Acta Crystallogr. D* **50,** 869–873.